Design of Autoland Controller Functions with Multi-Objective Optimization

Gertjan Looye*and Hans-Dieter Joos[†]

German Aerospace Center
DLR-Oberpfaffenhofen
Institute for Robotics and Mechatronics
D-82234 Wessling, Germany
E-mail: gertjan.looye@dlr.de

Abstract

The application of multi-objective optimization to the design of longitudinal automatic landing control laws for a civil aircraft is discussed. The control laws consist of a stability and command augmentation, a speed / flight path tracking, a glide slope guidance, and a flare function. Multi-objective optimization is used to synthesize the free parameters in these controller functions. Performance criteria are thereby computed from linear as well as nonlinear analysis (eg. simulations, eigenvalues). Robustness to uncertain and varying parameters is addressed via a multi-model approach, via robustness criteria (eg. gain and phase margins), and via statistical criteria (from on-line Monte Carlo analysis). For each controller function an optimization problem set-up is defined. Starting with the inner loops, the synthesis is sequentially expanded with each of these set-ups, eventually leading to simultaneous optimization of all controller functions. In this way, dynamic interactions between controller components are accounted for, and inner loops can be compromised such, that these can be used in combination with different outer loop functions. This reduces controller complexity while providing good over-all control system performance.

1. Introduction

The development of automatic landing (autoland) control laws for civil aircraft is a demanding task, since high safety standards have to be met before

---
*Research Engineer, Phd candidate
[†]Research Engineer, Phd

operational use under Cat IIIb conditions is allowed. The landing mission, consisting of glide slope tracking and flare/runway alignment shortly before touch down, is relatively straight forward. However, the autoland design task is complicated by the large amount of varying and uncertain parameters involved. In the first place, aircraft loading and configuration parameters (in this paper collected in the vector p_a) may vary for each landing case. Second, environment parameters (vector p_e), such as runway, approach terrain, ILS system, atmospheric, and wind characteristics are different for each landing, as illustrated in figure 1. For
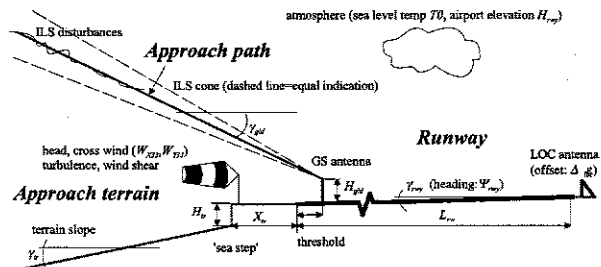

Figure 1: Typical parameters and disturbances during a landing

certification, autoland performance under varying aircraft and environment parameters has to be demonstrated via extensive Monte Carlo (MC) analysis, augmented with flight test validation [2]. The control designer also has to account for uncertain parameters in the aircraft design model to cover differences with the actual aircraft, or even with the high-fidelity and flight test-validated model used for final Monte Carlo assessment [11]. Autoland control laws consist of functions for glide slope and localizer hold, flare and runway align-

ment (in case of cross wind), and inner loops for stability and command augmentation. The design of these functions heavily relies on engineering skills (especially for architecture development), and may involve considerable trial-and-error in order to tune the controller parameters to meet design specifications. Important problems hereby are the large number of design criteria that have to be addressed in face of the afore mentioned varying/uncertain parameters, as well as the criteria themselves. Typical autoland design requirements, such as risk limits on touch down parameters, do not always translate easily into computational criteria that can be handled by commonly used controller synthesis methods.

In this paper, these problems are addressed by the application of a design process that is based on multi-objective optimization [3, 10]. This methodology involves so-called min-max optimization of free parameters (eg. gains, filter time constants) in a pre-defined controller structure with respect to a (possibly very large) number of computational criteria and constraints [4]. The controller structure has to be provided by the designer. However, this allows available experience and/or proven architectures to be (re-)used. The computational criteria may be obtained from linear as well as nonlinear analysis, and may be formulated directly from (in this case, autoland) design specifications. Varying and uncertain parameters can be addressed via a multi-model approach, via robustness criteria, or even statistical criteria obtained from on-line Monte Carlo analysis [10, 3].

In this paper it will be shown how these features can be exploited to tune free parameters (also called 'tuners', T) in a modular autoland control system for a small civil aircraft. The design process is depicted in figure 2. As a first step (A), the global architecture is defined. Detailed design of functions within this architecture is addressed in step B, involving detailed specification of the control law structure, and the formulation of function-specific computational criteria. The controller structures are integrated into the autoland system, which, in combination with the aircraft model, can then be used for closed loop analysis required for criteria computation.

The actual optimization of the controller functions is performed in step C. In this paper, a tuning strategy is developed that eventually allows all controller components to be optimized simultaneously. In this way, on one hand interactions between functions are accounted for that other-
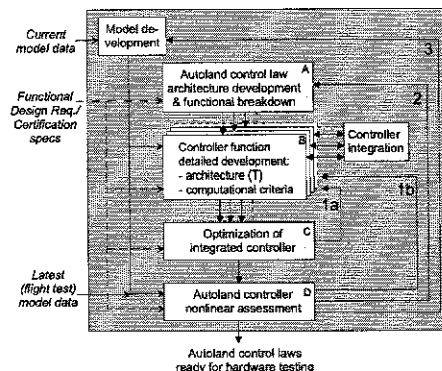

Figure 2: Optimization-based autoland control laws design process

wise have to be addressed by hand, and on the other hand, controller complexity can be reduced, because inner loop functions can be optimized in combination with multiple outer loop functions. This is demonstrated by tuning one set of inner loops for use with the glide slope, as well as the flare mode.

Performance and robustness of the resulting autoland system is assessed in step D of figure 2. The iteration loops 1A and 1B involve adjustments to computational criteria or component architectures, in case optimization or assessment results are not satisfactory, or in order to further improve them. In case of severe shortcomings, the overall controller structure may have to be reconsidered (loop 2). Loop 3 may be required in case of major model updates. However, by explicitly addressing model uncertainty in the process, this loop may possibly be avoided, see Ref. [11].

This paper is structured as follows. In section 2 the aircraft model is discussed briefly. In section 3 the controller architecture is described. In section 4 the optimization set-ups for the controller functions are discussed, in section 5 the actual optimization approach is described. In section 6 optimization results are discussed, and in section 7 conclusions are drawn.

2. The aircraft model

The aircraft is a VFW-614 ($\sim$ 30 passengers) called ATTAS (Advanced Technologies Testing Aircraft System), which has been configured as DLR's fly-by-wire test bed [1].

The model is based on the Newton-Euler equations of motion [14] for a rigid body. The aerodynamics are valid for the landing configuration and

include unsteady effects, ground effect, and interaction with the engine exhaust. Aerodynamic coefficients as well as the moments of inertia have tolerances of 10% (longitudinal parameters) or 30% (lateral parameters, ground effect). For example, the tolerance on the derivative of the aerodynamic pitching moment coefficient C_m with respect to the pitch rate q is written as:

$$C_{m_q} = C_{m_{q0}}(1 + \Delta C_{m_q})$$

where $C_{m_{q0}}$ is the nominal value, and ΔC_{m_q} is the tolerance. The vector containing all uncertain parameter tolerances in the aircraft model is p_u. The available controls are ailerons δ_A, elevator δ_E, rudder δ_R, and engine throttle settings $\delta_{TH1,2}$. The control surface actuators are linear, but rate and position limited. The turbofan engine dynamics and thrust computation are nonlinear. The fuel control unit shows backlash behavior, equivalent to several degrees of throttle input.

The wind model includes wind shear as present in the earth's boundary layer, Dryden gust filters (as specified in Ref. [2]), as well as additional parameterized wind shear models. For the atmosphere, approach terrain, runway and ILS equipment characteristics, parameterized (parameter vector p_e) models are included according to Ref. [2].

The model outputs are the measurements available to the control system: calibrated airspeed V_{cas}, true airspeed V_{tas}, ground speed V_g, body angular rates p, q, r, attitude angles ϕ, θ, ψ, load factors n_x, n_y, n_z, flight path angles χ, γ, angle of attack α, vertical speed V_Z, deviations from the ILS beam $\epsilon_{LOC}, \epsilon_{GS}$ (in mA), radio and barometric altitude H_{ra}, H_{baro}, and the mean fan shaft speed of both engines N_1. The sensor models are linear, but the output signals are quantized. The signals N_1, $\epsilon_{LOC}, \epsilon_{GS}$, and α are corrupted with noise. Finally, parameters p_a related to the aircraft configuration (e.g. the mass m, and the center of gravity location x_{CG}) may be assumed known to the controller.

3. The controller architecture (A,B)

The selected structure for the autoland controller is depicted in figure 3. It has previously been applied to a large transport aircraft, see Ref. [10]. Three main loops can be identified: Stability and Command Augmentation (SCA), Speed/Path Tracking (SPT), and guidance. Complexity of autopilot control laws may be considerably reduced by implementing only one component for each
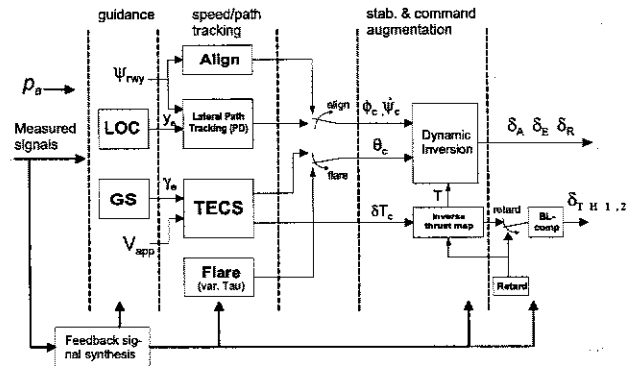

Figure 3: Autoland controller architecture (Remark: for block inputs, only command and error signals shown)

function only. This is an important feature of the Total Energy Control System (TECS) which is used as a SPT function: a single speed/flight path tracking control law can be used as the core of a complete set of longitudinal autopilot modes, see Refs. [6, 7]. In this autoland architecture, the same principle is applied to the Stability and Command Augmentation (SCA) function, which is used by all SPT functions, see figure 3. In this paper, we will only discuss the design of the longitudinal controller functions. These will be briefly described in the following. For more details, see also Ref. [10].

Inner loops
The task of the inner loops is to improve stability and to achieve robust tracking of command variables (ϕ_c, θ_c, ψ_c). The use of θ_c as inner loop command variable allows for direct control over the pitch attitude dynamics. Especially during flare, these play an important role in pilot acceptance. The inner loops were designed with Nonlinear Dynamic Inversion (NDI) [13]. Inverse model equations compensate the nonlinear aircraft dynamics, resulting in uniform and decoupled command responses, so that (manual) gain scheduling of the control laws is avoided. A detailed discussion on the inner loops can be found in Refs. [9, 8]. The closed loop dynamics are shaped using a linear outer loop control law:

$$\dot{q}_d = K_\theta(\theta_c - \theta) - K_q q$$

where $\dot{q}_d$ is the longitudinal reference input of the NDI controller, θ_c is the commanded pitch attitude angle, and K_θ and K_q are constant gains.

Longitudinal tracking and glide slope mode
For longitudinal speed and flight path tracking

during the approach, the Total Energy Control System (TECS) is used [6], see figure 4. The TECS-
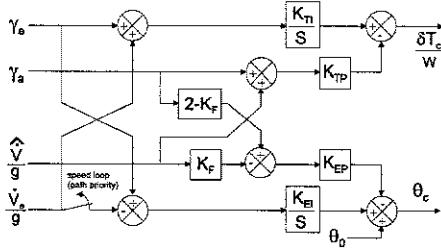

Figure 4: TECS controller structure (subscript e denotes an error from a commanded value)

architecture offers pilot-like decoupled tracking of speed and flight path angle commands. The input signals are air mass referenced flight path angle $\gamma_a \approx -V_Z/V_{cas}$ and filtered acceleration $\hat{\dot{V}}/g$. Here, TECS controls pitch attitude θ_c and thrust (per unit weight, $\delta T_c/W$). An inverse thrust map and an engine backlash compensation scheme (BLcomp) are used to generate appropriate throttle commands (figure 3). The gain K_F allows for shifting control priority to flight path tracking. The speed loop is opened in case thrust saturates. The feedback signal $\hat{\dot{V}}/g$ is obtained from complementarily filtering of the measured calibrated airspeed V_{cas} and the time derivative of the inertial speed $\dot{V}$ (computed from Inertial Reference Signals), with time constant τ_V [7]. The acceleration error $\dot{V}_e/g$ is computed from proportional feedback of the calibrated airspeed:

$$\dot{V}_e = K_V(V_{app} - V_{cas}) - \hat{\dot{V}}$$

where V_{app} is the selected approach speed.
The flight path angle error is computed in the Glide Slope mode [7]:

$$\gamma_e = \frac{1}{\hat{V}}\left[K_h\frac{1}{\tau_h s + 1}\Delta\tilde{h} - \hat{\dot{h}}\right] \qquad (1)$$

where $\hat{V}$ is a complementarily filtered speed signal, and $\Delta\tilde{h}$ is the height error estimated from the glide slope signal, which is filtered with time constant τ_h in order to remove high frequency signal noise. The estimated vertical speed with respect to the glide slope $\hat{\dot{h}}$ is obtained from complementarily filtering of $\Delta\tilde{h}$ and inertial reference signals (time constant is $\tau_{\dot{h}}$).

Flare law
For the flare law, the so-called variable Tau principle [5] was chosen (figure 5). It features constant

initiation height (H_{flare}) and low touch down dispersion under varying wind conditions. A feed forward part is added consisting of a ramp command to increase pitch (θ_{Ramp}) as well as the mean TECS attitude command $\hat{\theta}_0$, multiplied by K_{FW} (starting value is 1). The angle $\hat{\theta}_0$ is obtained by low-pass filtering θ_c commanded by TECS during the approach, and holding the value from flare initiation (figure 5).
The vertical speed $\hat{\dot{h}}$ is obtained by complementary filtering the radio altitude H_{ra} and V_Z, resulting in a runway referenced signal with low noise content. From the difference $\hat{\dot{h}} - (-V_Z)$ an additional feed forward command is generated via K_{RW}, anticipating a possible runway slope. During flare
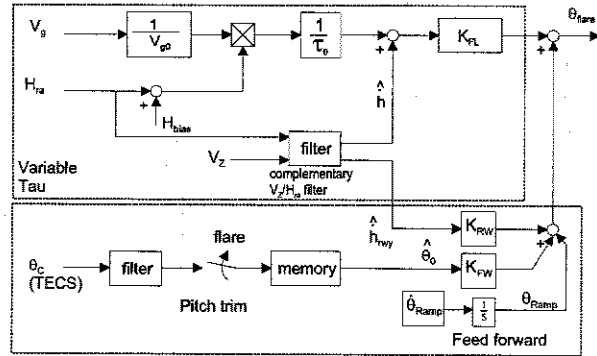

Figure 5: Flare architecture

the throttles are retarded at a constant rate $\dot{\delta}_{TH_c}$ (proportional to the ground speed at flare init), such that these reach idle position at touchdown.

4. Optimization problem set-ups (B)

For each individual controller function, an optimization problem set-up is defined. Such a set-up includes properties of the free parameters in the controller structure, computational design criteria (including properties such as scaling, type, etc.) that apply to the specific function, as well as macros and models to compute these criteria.

Stability and Command Augmentation (SCA)
The gains K_θ and K_q are tuning parameters for command shaping. Uncertain model parameters that also appear in the inverse model equations (p_u^*), can be effectively used as additional tuning parameters to improve robustness [9, 8]. The criteria for the longitudinal part of the NDI inner loop are listed in table 1. Those based on simulation 1

are intended for command shaping, those on simulation 2 for disturbance rejection, and those based on linear analysis are intended to guarantee closed-loop stability (over all eigenvalues, including zero dynamics) and stability robustness to unspecified modeling uncertainty (eg. time delays, unmodeled dynamics).

name	description	computation
Simulation 1, step: $\theta_c = 5$ deg, no turbulence		
THrt	rise time	see remarks
THos	over shoot	,,
THcontr	δ_E control activity	$\max_{t>1.2s}\{|\dot{\delta}_E|\}$
Simulation 2, heavy turbulence		
THturb	disturbance rejection	$\frac{1}{60}\int_{t=0}^{t=60}(\theta_c - \theta)^2 dt$
Linear analysis		
gmAD	gain margin at δ_E-act.	see remarks
pmAD	phase margin at δ_E-act.	,,
gmST	gain margin at θ-sens.	,,
pmST	phase margin at θ-sens.	,,
DAMPdi	min. damping (lon)	$\min\{\zeta_i\}$ (longitudinal)

Table 1: Criteria for inner loops. Remarks: All computations: symmetrical horizontal flight; altitude=1000 ft; nominal aircraft loading. Step times: $t_s = 1\ s$. Rise time: Δt between 10% and 90% of command. Gain/phase margins: as in [12].

In multi-objective optimization, relative importance of criteria is expressed via scaling. Especially in case of conflicting requirements, this gives the designer an effective means to make trade-offs and to set priorities. Scaled criteria have to be formulated such, that the objective is to minimize them, and that a value less than one is considered satisfactory.
Criteria scaling can be performed by division of each criterion by its demanded value:

$$\hat{c}_i(T) = c_i(T)/d_i$$

where $c_i(T)$ and d_i are the computed value and demanded value of criterion i respectively, and T denotes the current set of tuning parameters. Scaling can also be done using so-called 'good-bad' values [3]. Here, a special type of 'good-bad' scaling is used, as will be explained for $gmAD$ in figure 6. The demand is that the gain margin is at least 4 dB ('bad-low'). Any value larger than 6 ('good-low') is considered equally good and therefore scaled to 0. Below 6 dB, the scaled value increases linearly, such that a value of 1 is reached for the bad-low value of 4 dB. Any value between 4 and 6 dB is acceptable, any value lower than 4 dB is considered unacceptable (bad). As an example, if the gain margin is 3 dB, its scaled value equals 1.5. In the same fashion, 'good-high' and 'bad-high' values can be specified.
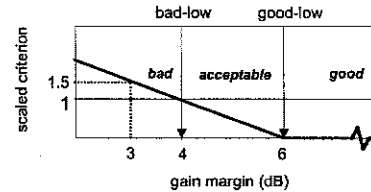

Figure 6: Scaling of $gmAD$ with good-bad values

The scalings applied to the SCA criteria are given in the first part of table 2 ($THrt\ ...\ DAMPdi$). Some of the criteria are treated as inequality constraints (i.e. $\hat{c}_i(T) \le 1$). For example, a rise time of 2.5 s is demanded. If this is satisfied, there is no point to further minimize this criterion, since this will unnecessarily go at the cost of stability and control effort.

Speed / flight Path Tracking (SPT) control laws
The task of the TECS controller is decoupled speed and flight path angle tracking, while providing adequate stability margin. These tasks are reflected by criteria that are computed from three nonlinear simulations and linear analysis, see table 3. Simulations 1 and 2 are intended for flight path angle and speed step response shaping. Simulation 3 is intended to assess turbulence rejection. The corresponding scalings are given in table 2. Those for damping and stability margins are as in table 2.

Of course, the SPT control laws always work via the SCA system. Thus, except for the TECS gains, also tuning parameters in the NDI controller affect the performance criteria in table 3.

Glide slope mode
For the glide slope mode again command shaping criteria are applied, see table 4 (simulation 1). A more important aspect during glide slope and approach speed tracking is disturbance rejection, whereas pitch attitude dynamics and throttle activity have to be limited for passenger comfort and pilot acceptance reasons. Design requirements were based on indicators listed in the second column of table 4. One possibility is to derive computational criteria from analytical covariance analysis. We tried a different approach, based on nonlinear approach and landing simulations performed in the on-line Monte Carlo analysis that is used to compute statistical flare law criteria (discussed in next subsection), see table 4. Since each landing is performed with different parameter vectors p_e, p_a, their variation is implicitly addressed

American Institute of Aeronautics and Astronautics

Crit. unit	Bad low	Good low	Good high	Bad high/ Dem.	
Longitudinal SCA criteria					
THrt (s)	–	–	–	2.5	c
THos (-)	–	–	–	0.05	c
THcontr (deg/s)	–	–	–	12.0	m
THturb (deg²)	–	–	–	0.08	m
gmAD (-)	–	–	4.0	6.0	m
pmAD (deg)	–	–	40	60	c
gmST (-)	–	–	4.0	6.0	m
pmST (deg)	–	–	40	60	c
DAMPdi (-)	–	–	0.6	0.7	c
Longitudinal SPT criteria					
GArt (s)	–	–	–	16.0	c
GAos (-)	–	–	–	0.1	c
GAst (deg)	–	–	–	0.2	m
THcmd (deg/s)	–	–	–	2.0	m
GAVA (m/s)	–	–	–	0.5	m
VArt (s)	–	–	–	20.0	c
VAos (-)	–	–	–	0.10	c
VAst (m/s)	–	–	–	0.5	m
dTHR (deg/s)	–	–	–	0.15	m
VAGA (deg)	–	–	–	1.0	m
NZturb (s⁻²)	–	–	–	0.007	m
THCturb (deg²)	–	–	–	0.167	m
THRturb (deg²)	–	–	–	5	m
Glide slope criteria					
GSrt (s)	–	–	–	20	c
GSos (-)	–	–	–	0.12	m
GSst (m)	–	–	–	2	c
maxGSdev (mA)	–	–	–	200	m
maxGSdev50 (mA)	–	–	–	200	m
meanGSdev (mA)	–	–	–	1	m
maxTHEdev (deg)	–	–	–	3	m
maxVCdev (m/s)	–	–	–	8.0	m
Flare criteria					
XTDnom (m)	360	380	400	420	m
VZTDnom (m/s)	-3.0	-2.8	-2.4	-2.2	m
THgrad (rad/s)	–	–	–	1	c
dHgrad (m/s)	–	–	–	1	c
dDEmax (deg/s)	–	–	–	10	c
meanHTP60 (m)	8	10	12	15	m
stdevHTP60 (m)	–	–	–	1.3	m
limHTP60 (m)	0	5	–	1	c
meanXTD (m)	300	350	400	450	m
stdevXTD (m)	–	–	–	75	m
limXTD (m)	–	–	–	680	c
meanVZTD (m/s)	-6	-4	-2	-1.5	m
stdevVZTD (m/s)	–	–	–	1.4	m
limVZTD (m/s)	–	–	–	3.1	c

Table 2: Scaling of all optimization criteria. Remark: c=inequality constraint, m=minimize, p=passive

in optimizing for disturbance rejection. Due to the large number of simulations involved, the risk that the optimizer may anticipate a specific noise signal, is reduced. The scalings on the criteria are given in table 2.

Flare mode
For the flare mode deterministic and stochastic criteria are considered. The deterministic criteria (table 5, 2) are computed from a nonlinear landing simulation. The stochastic criteria are computed from on-line Monte Carlo analysis. To this end, $n_{MC} = 400$ nonlinear landing simulations are per-

name	description	computation
Simulation 1, step: $\gamma_c = 3$ deg, no turb.		
GArt	rise time γ	see remarks table 1
GAos	over shoot γ	,,
GAst	'settling time' γ	$\max_{t>25s}\{|\gamma_c - \gamma|\}$
THcmd	θ cmd effort	$\max\{|\dot{\theta}_c|\}$
GAVA	max. speed deviation	$\max\{|\Delta V_{cas}|\}$
Simulation 2, step: $V_c = 10m/s$, $\gamma = -3$ deg, no turb.		
VArt	rise time V_{cas}	see remarks table 1
VAos	over shoot V_{cas}	,,
VAst	'settling time' V_{cas}	$\max_{t>25s}\{|V_c - \Delta V_{cas}|\}$
dTHR	throttle activity	$\max\{|\dot{\delta}_{TH1c}|\}$
VAGA	max. γ deviation	$\max\{|\Delta\gamma|\}$
Simulation 3, heavy turbulence: trimmed on glide slope, $V_{wind} = 15.4m/s$		
NZturb	load factor variation	$\frac{1}{60}\int_{t=0}^{t=60}\Delta n_z^2 dt$
THCturb	θ cmd effort	$\frac{1}{60}\int_{t=0}^{t=60}\Delta\theta_c^2 dt$
THRturb	throttle activity	$\frac{1}{60}\int_{t=0}^{t=60}\Delta\delta_{TH_c}^2 dt$
Linear analysis		
gmAD	GM δ_E-act.	see remarks table 1
pmAD	PM δ_E-act.	,,
gmSG	GM at γ-sens.	,,
pmSG	PM at γ-sens.	,,
gmSV	GM at V_{cas}-sens.	,,
pmSV	PM at V_{cas}-sens.	,,
DAMP	min. damping	$\min_i\{\zeta_i\}$

Table 3: Criteria for SPT loops. Remarks: Δ denotes deviation from trimmed value

formed in which all disturbances are applied. Before each landing simulation i_{MC}, 16 operational parameters ($\in p_a$, $\in p_e$, see figure 1) are selected randomly, according to prescribed statistical properties. After completing the simulations, the mean values and standard deviations of so-called risk-parameters are determined. The longitudinal risk parameters are: the height of the main gear over the runway at 60 m from the threshold (HTP60), to assess the risk of short landings, the runway touchdown distance from threshold (XTD), to assess the risk of long landings, and the vertical speed with respect to the runway surface (VZTD), to assess hard landings. From the mean values and standard deviations, the distribution and cumulative distribution functions can be computed, assuming that these are Gaussian. Based on JAR-AWO specifications, each risk parameter has a limit value for which the probability of exceedance must be proven to be less than 10^{-6} (average risk analysis).

For each of the risk parameters, the mean value, standard deviation, and probability of exceeding the limit value are addressed via optimization criteria [10], see table 2 (below). The probability criteria are addressed indirectly, as will be illustrated via an example. The limit value for X_{TD} is 915 m. As optimization criterion, the actual value of

Table 4: Criteria for Glide Slope mode.

name	description	computation
Simulation 1, offset of 50 m above glide slope, aircraft trimmed parallel to the GS, no turbulence.		
GSrt	rise time	see remarks table 1
GSos	over shoot	$\max_{t>30s}\{|H_{offset}|\}$
GSst	'settling time'	
Monte Carlo simulations, all effects (eg. turbulence, nonlinearities) included		
maxGLDdev	max. abs. vertical deviation from GS	$\max_{i_{mc}}\{\max_{10s<t<t_{fl}}\{|\epsilon_{GS}(t)|\}\}$
maxGLDdev50	abs. vert. dev. from GS, at flare init	$\max_{i_{mc}}\{|\epsilon_{GS}(t_{fl_{iMC}})|\}$
meanGLDdev	mean deviation from GS	$\sum_{i=1}^{n_{mc}}\int_{t=10}^{t_{fl_{iMC}}}\epsilon_{GS}(t)dt/\sum_{i=1}^{n_{mc}}(t_{fl_{iMC}}-10)$
maxTHEdev	max pitch angle dev. from mean value	$\max_{i_{mc}}\{\max_{10s<t<t_{fl}}\{|\theta(t)-\bar{\theta}|\}\}$
maxVCdev	max. speed deviation	$\max_{i_{mc}}\{\max_{10s<t<t_{fl}}\{|V_{app_{iMC}}-V_{cas_{filt}}-0.5m/s|\}\}$

Table 4: Criteria for Glide Slope mode. Remarks: n_{mc} =total number of Monte Carlo simulations, i_{mc} = index of individual MC simulation, $t_{fl_{iMC}}$ = flare initiation time for simulation i_{mc}, ¯ indicates mean value for $10s < t < t_{fl_{iMC}}$, $V_{cas_{filt}}$ is V_{cas} filtered with 5 s time constant.

XTD for which the probability of exceeding equals 10^{-6} is taken:

$$X_{TD_{lim,6}} : P(X_{TD} \geq X_{TD_{lim,6}}) = 10^{-6}$$

$X_{TD_{lim,6}}$ (found by interpolation) is divided by its demanded value of 915 m and handled as an inequality constraint $(X_{TD_{lim,6}}/915 < 1)$. This is equivalent to demanding $P(X_{TD} > 915) < 10^{-6}$. However, in order to achieve more margin (or, lower probability of exceedance), the demanded value has been set to 680 m, or: $X_{TD_{lim,6}}/680m < 1$, so that $P(X_{TD} > 915) << 10^{-6}$.

5. Controller optimization (C)

For tuning the autopilot functions, the multiobjective optimization environment MOPS (Multi-Objective Parameter Synthesis [3]) is used. MOPS allows multiple optimization tasks (setups), as defined in the previous section, to be

Name	Specification description	Computation
Simulation 1, nonlinear simulation, no disturbances, nominal conditions		
XTDnom	touchdown point	$x_{td}(t_{td})$
VZTDnom	vert. touchdown speed	$\dot{H}_{ra}(t_{td})$
THgrad	$\dot\theta$ may not change sign	$1 - \min_{t_1 \leq t \leq t_{td}}\{\dot\theta(t)\}$
dHgrad	$\dot{V}_Z$ may not change sign	$1 + \max_{t_1 \leq t \leq t_{td}}\{\dot{V}_Z\}$
dDEmax	elev. rate	$\max_{fl \leq t \leq t_{td}}\{|\dot\delta_E|\}$
t_{td} = touchdown time, t_1 = flare init time + 2 s		

Table 5: Deterministic flare criteria

comfortably combined into a single one. This feature allows for tuning controller functions simultaneously, as will be described shortly.

In section 4, for each controller function an optimization set-up has been defined. Optimizing each function independently does not guarantee sufficient performance of the complete system, since in spite of time scale separation between sequential loops, considerable dynamic interaction may be left. This especially holds for the SCA in combination with the flare and SPT functions. For this reason, the intention is to tune all controller functions simultaneously. However, in order to steer the optimization process in a structured way, and to keep an overview over the large amount of criteria, simultaneous optimization is not performed in one shot. Instead, tuning is started with the SCA inner loop, and then sequentially expanded with the problem set-ups for SPT and guidance functions. The tuning process is depicted in figure 7.
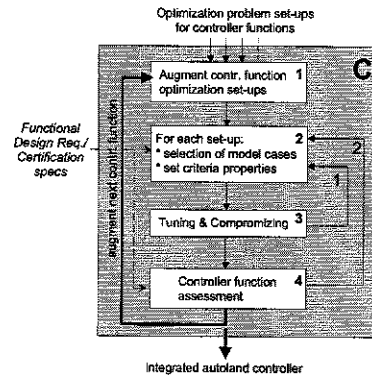

Figure 7: Optimization-based autoland control laws design process (step C in figure 2)

For a combined optimization task (step 1), criteria properties (scaling, type) are adjusted and, if de-

sired, multiple model cases are selected (step 2). The latter allows for compromizing performance for nominal and worst-case model parameter combinations (p_e, p_u, p_a) and is therefore an effective means to address performance robustness [3]. After tuning and compromizing via multi-objective optimization in step 3 (to this end, several optimization algorithms are available in MOPS), performance and robustness of the resulting controller functions is assessed (step 4). After optimization or assessment, the designer may decide to adjust criteria scaling (loop 1,2) in order to influence compromize solutions. In case of robustness problems, worst model cases may be added to the optimization (loop 2). In case the result is satisfactory, the next controller function set-up is added (step 1). Eventually, all controller functions are optimized simultaneously.

As already mentioned, the SCA inner loop function is tuned first. Since dynamic inversion is sensitive to modeling errors, special attention has to be paid to this issue[9]. Robustness to parametric uncertainty (p_u) can be addressed by including multiple model cases in the optimization, while the same parameters appearing in the inverse model equations (p_u^*) are used as additional tuners [9, 8]. For the longitudinal case however, keeping p_u^* at nominal values provided sufficient robustness. For this reason, it was decided to proceed with the nominal model only. The linear controller parameters (in this case K_θ, K_q) are used for command shaping. The optimized values are used as a start for the following step.

Next, the optimization set-up for the TECS-based flight path and speed tracking loop is added. The SCA set-up is retained, but the critical criteria are changed into inequality constraints (step 2 in figure 7). During optimization the inner loop gains K_θ, K_q may thus be adjusted to improve TECS performance, but the optimizer is prevented from distorting the achieved SCA performance by choosing gains K_θ, K_q that are only valid with TECS connected. Again, the newly optimized parameters are used as a start for the following step. Next, the glide slope mode is added to the optimization. Criteria of the TECS set-up are also set as inequality constraints. At this point, the Monte Carlo based criteria are left out, since their computation is too time consuming for an intermediate optimization step. During tuning of the glide slope mode it became clear that tight path tracking was hard to achieve. Fortunately, in the TECS structure the gain K_F (normally 1) can be used to

(temporarily) swift priority to flight path tracking. Opening the speed loop (see figure 4) is also helpful. The parameter K_F may be adapted when the glide slope mode is connected. Evaluation of the criteria for TECS alone (as in previous optimization) is performed for $K_F = 1$ and the speed loop closed. Regarding tracking, the glide slope mode is most demanding. It is expected that other autopilot modes can be added later on, without, or with only minor adjustment of TECS gains.

Finally, the flare mode is added, including Monte Carlo based criteria. Those related to the glide slope criteria are activated as well now (table 4). The optimization task now includes all longitudinal autoland functions. All gains may be adjusted, and all criteria (see section 5) are active. Those in the SCA and TECS set-ups are set as inequality constraints. This on one hand allows these functions to be adjusted to improve outer loop performance, but on the other hand prevents distortion of performance of the functions without the flare or GS mode connected.

	Active tuner:	Augmented design set-up: (set-up to the left is retained)				unit
		SCA	TECS	GS	flare	
SCA	K_θ	1.6	2.0	2.0	2.1	s^{-1}
	K_q	2.5	3.2	3.2	3.3	s^{-1}
SPT (TECS)	K_{EI}		0.2	0.3	0.2	$s^{-1}rad$
	K_{TI}		0.4	0.3	0.43	$s^{-1}rad^{-1}$
	K_{EP}		0.56	0.4	0.33	rad
	K_{TP}		0.6	1.0	1.2	rad^{-1}
	K_V		0.12	0.12	0.12	s^{-1}
	K_F		*1.0	1.0	0.28	−
	τ_V		*10	*10	8.8	s
GS	K_h			0.06	0.06	s^{-1}
	τ_h			2.5	2.6	s
	$\tau_{\dot h}$			15	3.9	s
Flare	K_{FL}				-0.04	$rad(m/s)^{-1}$
	H_{bias}				1.4	m
	θ_{Ramp}				0.18	−
	K_{PW}				1	−
	K_{RW}				0.12	$rad(m/s)^{-1}$
	H_{retard}				6.0	m
	H_{flare}				12.1	m

Table 6: Development of tuner parameter values. '*' = inactive

6. Controller optimization results

In this section, we will assess the performance of the final controller, as well as intermediate results. Figure 8 shows the result of the optimization in so-called parallel co-ordinates. All scaled criterion values have been plotted on an individual axis and connected through a line (i.e. one graph corresponds to one tuning parameter set T). The
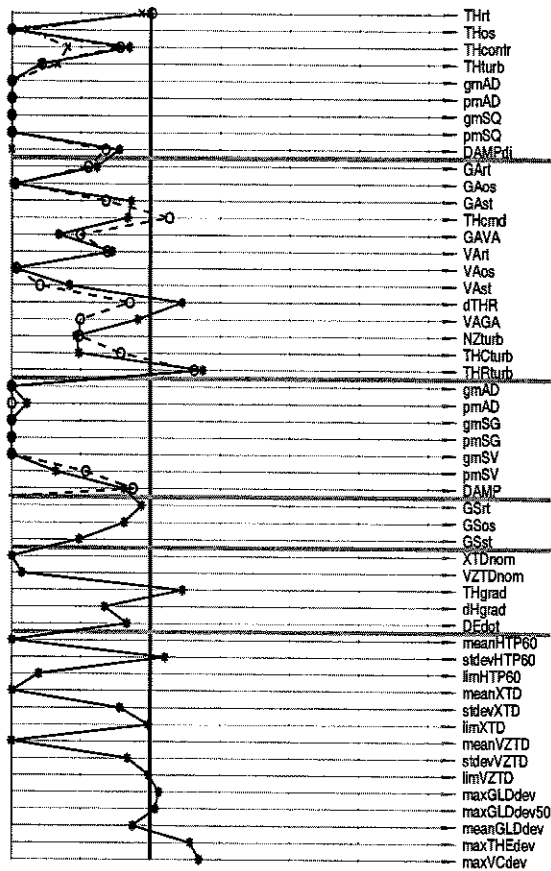
American Institute of Aeronautics and Astronautics

Figure 8: Criteria in parallel co-ordinates (rotated 90 deg clockwise): '-.' = SCA optim., '- -' = SCA+SPT optim., '–'=complete optimization

fat horizontal line indicates a value of one. Criteria values below this line are considered satisfactory. Parallel co-ordinates are standard graphical output during optimization, giving quick insight in the optimization progress, in criteria that are hard to satisfy, and in criteria that conflict and thus have to be compromised [3]. We will use the representation to compare the intermediate optimization steps. Criteria vectors belonging to the different optimization set-ups have been separated by thick vertical lines.

The dash-dotted line (marker 'x') in figure 8 represents the result after optimization of the SCA function. The other set-ups have not been involved yet, so that the line can only be drawn for the SCA criteria. The resulting tuner parameter values can be found in the first column of table 6. Since all scaled criteria values are below 1, the result is regarded satisfactory. The corresponding
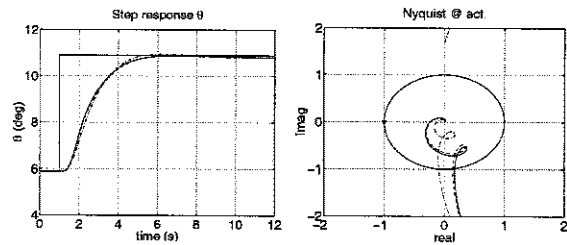

Figure 9: SCA results (for legend, see caption of figure 8)

pitch attitude command response and the Nyquist curve for the loop opened at the elevator actuator have been plotted in figure 9 (dash-dotted curves). The phase margin is 85 deg, which is larger than the good-low value of 60 deg (table 2) demanded for $pmAD$. As depicted in figure 8 on the $pmAD$ axis, the scaled criterion value is thus 0 (note that this is the case for all linear criteria).

The result of the combined optimization of the SCA and SPT function is represented by the dashed line. This time, the curve can be drawn for the parallel co-ordinates up to $DAMP$ (dashed line, marker 'o'). The resulting tuning parameter values can be found in the second column of table 6. All scaled criteria values are below one, except for $THcmd$ and $THRturb$ (control activity). However, exceedance with 20 and 40% was considered acceptable, since these criteria were not considered critical. Corresponding step responses on γ_a and V_{cas} can be found in figure 10 (dashed lines). Due to further adjusting K_θ and K_q, SCA criteria values have changed, see figure 8. $THrt$ increased somewhat, but not beyond 1 (i.e. rise time < 2.5s), since the criterion was set as an inequality constraint in the optimization. Damping ($DAMPdi$) and control effort ($THcontr$) have deteriorated, but are still acceptable (< 1).
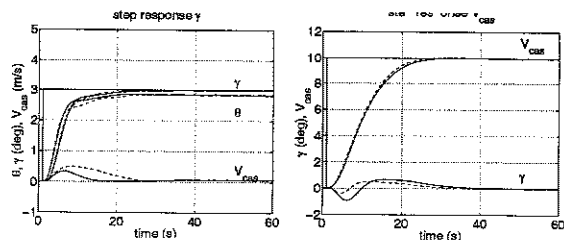

Figure 10: TECS results (for legend, see caption of figure 8)

Results of the combined optimization of SCA,

9

SPT, and GS set-ups will not be discussed (third column of table 6). Instead, we move on to the final optimization step, involving all set-ups augmented into a single optimization task. The result is represented by a solid line in figure 8 (marker '*'). The corresponding tuner parameter values can be found in the fourth column of table 6.
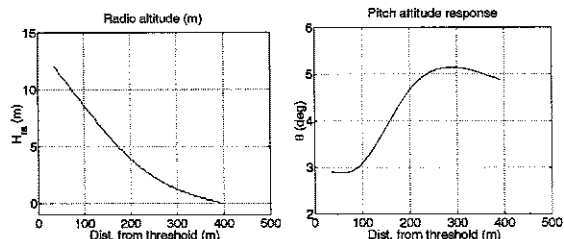

Figure 11: Flare results

Regarding the nominal flare manoeuver (figure 11), all criteria (*XTDnom ... DEdot*) are satisfactory, except for *THgrad* (table 5). It turned out that a slight nose drop during the flare (0.3 deg) had to be tolerated, unless considerable emphasis was put on feed-forward. This however made it hard to meet Monte Carlo assessment criteria that will be discussed shortly. At this point, architectural modifications may be necessary to further improve the design.

The maximum over-all deviation (maxGLDdev) and maximum deviation 50 m before threshold (maxGLDdev50) under turbulent conditions were difficult to improve beyond the criteria values shown in figure 8 (scalings had to be relieved as well, see table 2). Inspection of individual landings from the Monte Carlo analysis revealed that these maximum values occurred during extreme wind shears (>9 ft/s), caused by a combination of heavy turbulence and the standard wind profile as a function of height [2]. In further tuning, such cases should be eliminated. The TECS related parameters have been considerably modified during the final optimization step. Clearly, pitch attitude commands (*THcmd*) have decreased, at the cost of throttle activity (*dTHR*). This is related to minimizing pitch attitude excursions during glide slope tracking (*maxTHEdev*). However, the latter criterion was most difficult to improve. Again, it turned out that the maximum deviations occurred during heavy wind shears. Regarding the SCA related criteria, these slightly, but acceptably, deteriorate due to further adjustments of K_θ and K_q. The step response and Nyquist curve (solid) in figure 9 confirm this.

The most important criteria for certification are based on risk analysis from Monte Carlo assessment. The optimized result can be found in figure 12. The left half of the figure shows distribution of the risk parameters HTP60, XTD, and VZTD computed from the mean and standard deviations over 2000 landings (during optimization, only 400 were used). To the right the resulting cumulative distributions can be found. As an example for interpretation, the probability of landing at a sink rate (VZTD) higher than 2 m/s is $10^{-2.4}$, as indicated in figure 12. The graph should stay outside the shaded area, so that the probability of landing harder than 3 m/s (for ATTAS) is less than 10^{-6} (risk to be demonstrated). This has clearly been achieved by the optimizer. Incorporating these statistical criteria in the optimization was found extremely useful, since JAR-AWO robustness criteria could be addressed (and fulfilled) directly.
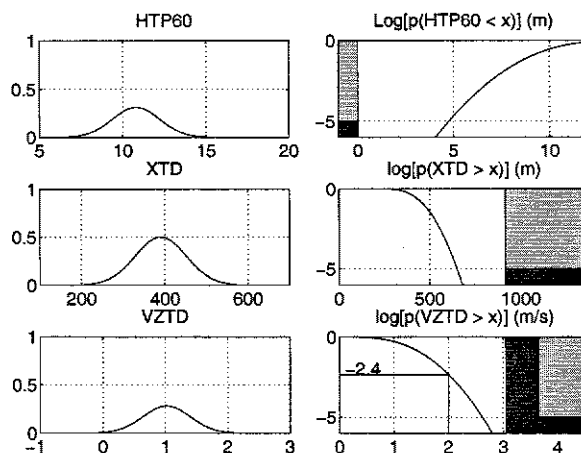

Figure 12: Monte Carlo simulation results

7. Conclusions

The design of longitudinal functions for an automatic landing system was presented. A tuning strategy for a modular control law architecture has been discussed, leading to simultaneous optimization of all controller functions. In this way, interactions between functions are accounted for, and the tuning of the Stability and Command Augmentation (SCA) structure could be compromised, so that it performs well with each outer loop function interconnected. This on one hand results in good performance of the over-all system, and on

the other hand reduces controller complexity. Currently, the Speed and flight Path Tracking (SPT) controller is only used by the glide slope mode, but the system may be extended with other autopilot modes, sharing the same SPT and SCA functions. Varying parameters (p_e, p_a) that influence the landing have been addressed in the controller architecture, as well as via criteria computed from on-line Monte Carlo analysis. Specifically, known aircraft parameters (p_a) are, to a large extent, automatically compensated by the Dynamic Inversion inner loops. Handling of uncertain parameters (p_u) has not been discussed in detail. This can be effectively done via a multi-model approach, as demonstrated for the Dynamic Inversion-based SCA function in Ref. [9]. Robustness to unspecified uncertainty has been addressed via stability margins as optimization criteria.

Multi-objective optimization has proven to be very powerful to address system performance and robustness using various types of criteria. Finding a global optimum solution is not guaranteed, but any result that satisfies demanded criteria values (specified via scaling) can be regarded as an acceptable candidate solution.

Obviously, performance can be further improved by enhancing the controller structure. The structure used in this design was successfully flight tested in September 2000, see Ref. [1]. The formulation of design requirements can also be improved. For example, SISO stability margins are to be replaced with multivariable ones. The glide slope disturbance rejection criteria did not work to full satisfaction, and therefore should be further enhanced.

Acknowledgments

References

[1] M. Bauschat, W. Mönnich, D. Willemsen, and G. Looye. Flight testing Robust Autoland Control Laws. In *Proceedings of the AIAA Guidance,*

Navigation and Control Conference 2001, Montreal CA, 2001.

[2] Joint Aviation Authorities Committee. Joint Aviation Requirements, All Weather Operations. Technical report, JAAC, 1996.

[3] H.-D. Joos. A methodology for multi-objective design assessment and flight control synthesis tuning. *Aerospace Science and Technology*, 3(3):161–176, April 1999.

[4] Hans-Dieter Joos. *In: J.F. Magni, S. Bennani, J. Terlouw, Eds. Robust Flight Control, a Design Challenge.*, chapter Multi-Objective Parameter Synthesis (MOPS), pages 13 – 21, 199 – 217. Lecture Notes in Control and Information Sciences, Vol 224. Springer-Verlag, 1997.

[5] A A. Lambregts. Avoiding the pitfalls in automatic landing control system design. *AIAA Paper 82-1599*, 1982.

[6] A A. Lambregts. Integrated system design for flight and propulsion control using total energy principles. *AIAA Paper 83-2561*, 1983.

[7] A A. Lambregts. Vertical flight path and speed control autopilot design using total energy principles. *AIAA Paper 83-2239*, 1983.

[8] Gertjan Looye. Design of Robust Autopilot Control Laws with Nonlinear Dynamic Inversion. *at – Automatisierungstechnik*, 49(12), 2001.

[9] Gertjan Looye and Hans-Dieter Joos. Design of Robust Dynamic Inversion Control Laws using Multi-Objective Optimization. In *Proceedings of the AIAA Guidance, Navigation and Control Conference 2001, Montreal CA*, 2001.

[10] Gertjan Looye, Hans-Dieter Joos, and Dehlia Willemsen. Application of an Optimisation-based Design Process for Robust Autoland Control Laws. In *Proceedings of the AIAA Guidance, Navigation and Control Conference 2001, Montreal CA*, 2001.

[11] G.H.N. Looye, C.E.S. Sancho, A.A. Makdoembaks, and J.A. Mulder. Design of Robust Autoland Control Laws using μ-Synthesis. In *Proceedings of the AIAA Guidance, Navigation and Control Conference 2002, Monterey CA*, 2002.

[12] The Math Works Inc. *Control System Toolbox, For Use with MATLAB – User's Guide*, January 1998.

[13] Jean Jacques E Slotine and Weiping Li. *Applied Nonlinear Control*. Prentice Hall, Englewood Cliffs, N.J., 1991.

[14] Brian L. Stevens and Frank L. Lewis. *Aircraft Control and Simulation*. Wiley-Interscience Publication. John Wiley & Sons, Inc., New York, 1992.